Zr-O-N coatings for decorative purposes: Study of the system stability by exploration of the deposition parameter space

C.I. da Silva Oliveira, D. Martinez Martinez, L. Cunha, M.S. Rodrigues, J. Borges, C. Lopes, E. Alves, N.P. Barradas, M. Apreutesei

PII: S0257-8972(17)31203-3
DOI: doi:10.1016/j.surfcoat.2017.11.056
Reference: SCT 22904

To appear in: *Surface & Coatings Technology*

Received date: 30 June 2017
Revised date: 14 November 2017
Accepted date: 20 November 2017

Please cite this article as: C.I. da Silva Oliveira, D. Martinez Martinez, L. Cunha, M.S. Rodrigues, J. Borges, C. Lopes, E. Alves, N.P. Barradas, M. Apreutesei , Zr-O-N coatings for decorative purposes: Study of the system stability by exploration of the deposition parameter space. The address for the corresponding author was captured as affiliation for all authors. Please check if appropriate. Sct(2017), doi:10.1016/j.surfcoat.2017.11.056

Zr-O-N coatings for decorative purposes: study of the system stability by exploration of the deposition parameter space.

C.I. da Silva Oliveira[1,], D. Martinez Martinez[1], L. Cunha[1], M.S. Rodrigues[1], J. Borges[1], C. Lopes[1], E. Alves[2], N.P. Barradas[3], M. Apreutesei[4]*

[1]*Center of Physics, University of Minho, Campus de Azurem, 4800-058 Guimaraes, Portugal.*

[2]*Instituto de Plasmas e Fusão Nuclear, Instituto Superior Técnico, Universidade de Lisboa, Bobadela LRS, Portugal.*

[3]*Centro de Ciências e Tecnologias Nucleares, Instituto Superior Técnico, Universidade de Lisboa, Bobadela LRS, Portugal.*

[4]*INSA de Lyon, MATEIS Laboratory, Villeurbanne, France.*

*Corresponding author: catarina.silva.oliveira@outlook.pt

Abstract

The deposition of decorative coatings is an excellent solution to modify the surface of any material, particularly the aesthetic finishing, without altering the properties of the substrate. Transition metal oxynitride films are interesting for many applications, due the simple and economic way to tune between nitride and oxide bonding. In reactive sputtering, this is done by playing with the flows of N_2 and O_2, leading to variations of properties (e.g. color) in different directions. In this paper, zirconium is selected as transition metal due to combination of different characteristics (color, biocompatibility, mechanical properties, corrosion resistance).

The literature about Zr-O-N films reveals a confinement of chemical composition. Therefore, the aim of this work is the exploration of the deposition parameter space in order to evaluate the stability of the Zr-O-N system, i.e. verify if the chemical composition of the films still falls in the same range after variation of different deposition parameters. To do that, a series of Zr-O-N films is deposited first at different reactive flows, maintaining the remaining deposition parameters constant. The obtained films can be classified in three different groups, based on their chemical composition, crystalline structure, and film growth. These groups can be successfully explained according to the sputtering characteristics, and correlated with the mechanical properties and color of the films measured by nanoindentation and spectrophotometry receptivity. The films deposited by variation of other

parameters are introduced afterwards and their characteristics are compared with the reference series.

Keywords: decorative, oxynitride, XRD, zirconium, RBS, aesthetic

1. Introduction

Bulk materials may fail to provide all the properties desired for a certain application (mechanical, optical, electrical…) [1]. Coatings are a reliable method to modify the surface of the materials in order to achieve those properties without modification of the underlying substrate [1]. In that regard, color is interesting for many consumer products were the aesthetics is a fundamental requirement, for instance for jewelry, eyeglass frames, wristwatch casings and wristbands, bathroom hardware (taps, towel racks, etc.), door locks and handles, among others [2–4]. These coatings, whose aesthetics function is important, are called decorative coatings and they should provide also scratch-resistance, and protection against corrosion, among other properties [2–4].

During a certain period of time, decorative coatings have been largely based on elementary materials and binary nitrides (TiN, HfN, ZrN…) [3]. Although transition metal nitrides exhibit outstanding optical and mechanical properties, there is a high restriction in the attainable color tones, particularly golden yellows, greys, and black [2, 3, 5]. More recently, transition metal oxynitrides have been gaining importance in the domain of decorative applications. This class of materials is particularly interesting because the properties of the films can be tuned between those of nitrides and those of oxides [2, 6–11].

In that regard, zirconium oxynitride coatings have been drawing attention over the past years, due to the combination of a wide palette of attainable colors [12–14], good biocompatibility [15], mechanical properties [16] and corrosion resistance [17, 18]. The majority of Zr-O-N films in literature have been deposited by reactive magnetron sputtering operated with different sources (DC, RF or pulsed-DC) [3–6, 8, 9, 13, 14, 19–46], and their properties have been typically tuned via the modification of reactive atmosphere [3–6, 8, 9, 13, 14, 19–25, 27–42]. As a result, the reported chemical composition of the Zr-O-N films is surprisingly limited located in a region of the Zr-O-N ternary diagram which lies between metallic Zr and Zr nitrides (ZrN and Zr_3N_4) and the region connecting nitrides, oxinitrides (ZrO_xN_y) and oxides (ZrO_2)

The aim of this work is to evaluate the observed stability of the Zr-O-N system. Therefore, we study the potential of other deposition parameters, e.g. target current

or bias, to modify the chemical composition, crystallographic phases and properties of Zr-O-N films. To do that, a series of samples prepared with different flows of a mixture of N_2+O_2 is deposited and characterized first, as a reference to evaluate the influence of the variation of other deposition parameters.

2. Experimental details

Zr-O-N thin films were deposited onto (111) silicon pieces (1.5 cm × 1.5 cm), glass (2 cm × 2 cm) and mirror-polished high-speed steel cylindrical substrates (∅=3 cm × 0.5cm) by reactive direct current magnetron sputtering in a laboratorial size deposition equipment. The substrates were first cleaned with alcohol and etched in a Zepto Plasma System (Diner) equipped with a 40 kHz / 100 W generator. During the etching process, the power used was 100 W and the Ar pressure was approximately 80 Pa. For the depositions, the substrates were clamped in a rotating holder (5 rpm) placed at 75 mm from the magnetron head. The base pressure was always below 2.6×10^{-3} Pa. The depositions were performed by sputtering a Zr target (99.6 % at., 100×200×6 mm^3) using Ar as working gas and a mixture of N_2 and O_2 (85:15) as reactive gases, respectively. The discharge parameters (target potential, applied current and work pressure) were monitored during the deposition using a Data Acquisition/Switch Unit by Agilent 34970A. The data was acquired with a Benchlink Data Logger III software. The substrates were not intentionally heated during film deposition.

The conditions used in the depositions of the Zr-O-N samples are listed in Table 1. The initial group of samples was deposited with reactive gas flows from 2.5 to 15 sccm maintaining the remaining conditions constant (Ar flow 25 sccm, Zr target current 2 A, no bias and 60 min. of deposition time). The other samples were deposited with similar conditions as this first group while varying one of the deposition parameters in order to investigate its effect in the characteristics and properties of the film. The labelling of the films indicates this situation; thus, samples belonging to the first group are identified only with the mixture flow, while samples from the second group are labelled with the mixture flow followed with the varied parameter and its value.

The morphology and thickness of the films was characterized by scanning electron microscopy (SEM) in an FEI - Nova 200 NanoSEM (FEG/ESEM) equipment operating at 10 kV. The chemical composition of the films was determined by Rutherford backscattering spectrometry (RBS), using CTN/IST Van der Graaff accelerator in a chamber where three detectors were installed: a standard PIPS detector at 140º, and two pin-diode detectors located symmetrically to each other both at 165º. The spectra were collected for 2 MeV $^{4}He^{+}$ beam and the angle of incidence was 0º (normal incidence). The compositional profile of the samples was determined using the software IBA Data furnace NDF v9.6d. The areal density of the films (RBS thickness in at/cm^2) has been also calculated, which can be transformed into density using the thickness measured by SEM [47]. The crystallographic structure was investigated by X-ray diffraction in grazing incidence at θ=4º on a Brucker D8 Advanced system apparatus using Cu K_α radiation (λ= 0.154 nm). Spectrophotometry was performed using a commercial Minolta CM-2600d portable spectrophotometer (wavelength range: 400–700 nm) in order to quantify the color of the samples according to CIELab 1976 color space [48]. The specular component has been included, and a small mask of 3 mm diameter has been used. The mechanical properties of some selected films were measured with a Nano Test nanoindenter (Micro Materials) using a conventional Berkovich indenter. The maximum load was selected in such a way that the maximum indentation depth did not exceed the 10%-15% of the coating thickness in order to avoid the influence of the substrate. The hardness and reduced Young's modulus were calculated from the load-unload displacement curves using the Oliver and Pharr method [49]. The spectrophotometric measurements were carried out in films deposited in Si, steel and glass in the same batch, while the rest of characterization was carried out in films deposited on silicon.

3. Results and discussion

3.1. Variation of the N_2+O_2 flow: sputtering zones

Figure 1 shows the influence of the flow of reactive mixture on the deposition pressure and target voltage (Figure 1a), deposition rate (Figure 1b), and chemical composition (Figure 1c) of the produced films. Table 1 includes two different values

of thickness evaluated by SEM and by RBS, which show similar trends. When both data were available, the density of the film could be calculated. The values are located between 4.87 and 6.27 g/cm^3, while the densities of metallic hexagonal Zr (h-Zr), metallic cubic Zr (c-Zr), cubic nitride (c-ZrN), cubic oxynitride (c-Zr_2ON_2) and monoclinic oxide (m-ZrO_2) are 6.52, 6.41, 7.09, 5.78 and 5.68 g/cm^3, respectively.

The deposition pressure obviously grows with the flow of reactive mixture (Figure 1a), although small 'jumps' can be observed, which indicate the transition between different regimes. Three different zones can be found, in agreement with a reactive sputtering process. Such finding is in line with what was reported by several works [8, 12, 13, 20, 21, 34], which identified three zones that can be labelled as metallic (M), transition or reactive (R), and oxide or poisoned (P). The classification of samples according to different groups is indicated in the right columns of Table 1.

Zone M corresponds to reactive gas flows up to 3.75 sccm. This zone includes the coatings with low target voltages (< 280 V) and high deposition rates (> 1.4 μm/h). These films have the highest concentration of Zr (> 68%) and very low amount of O (~1%), while the N/O ratio is higher than 10. Within this Zone, the increase of the N_2+O_2 flow caused a parallel reduction of deposition rate and Zr content. In addition, following the higher concentration of N, the density increases from 5.41 to a maximum of 6.27 g/cm^3 (film F3.75) which is in line with the higher density of the c-ZrN relatively to the densities of h-Zr and c-Zr.

The opposite behaviour is shown by samples belonging to Zone P (reactive gas flows above 4.7 sccm). These samples present a very similar deposition rate (around 0.6 μm/h) which is considerably lower than the values of the Zone M. The increase in the reactive gas flow leads to an increase of the target potential from values around 307 to values around 362 V. In this Zone the atomic concentrations of Zr, O and N are 46±3%, 18±3%, and 36±1%, respectively. The N/O atomic ratio is below 2.5, and the density of the films is lower than in film F3.75, in agreement with the lower densities of the phases including oxygen.

The Zone R (flows between 3.75 and 4.5 sccm), shows a intermediate behavior in terms of deposition rate, target voltage and O content. Thus, the O concentration has a value of 12±1%, which is significantly higher than in Zone M and lower than in Zone P. The Zr content is 44±1%, which is considerably lower than the

concentration of Zone M and very similar to Zone P. Finally, this Zone shows higher N concentrations than in the other two Zones, with values of 43±2%, which is similar to the Zr concentration. The N/O ratio is higher than 3. The density is intermediate between film F3.75 and samples from region P.

The behavior of the deposition rate and target pontential can be related to the composition of the sputtering atmosphere in the chamber; at low reactive flows, the poisoning of the target is overcomed by the cleaning caused by sputtering, and a strong metal flux arives to the substrate leading to higher deposition rates. When the reactive gas flow is increased, the poisoning rate increases relatively to the cleaning rate, and as a consequence, the poisoning of the target surface starts to take place. This causes an increase of the target potential and a reduction of the deposition rate, since the sputtering yield from a poisoned surface is lower.

In addition to the previous factors, the chemical composition of the films is also related to the gas composition of the mixture (poorer in O_2, 15%) and the relative affinity of both gases towards Zr (oxygen is more reactive with zirconium than nitrogen) [12]. In zone M, poisoning leads to high Zr contents. The low O content and increasing N concentrations for higher N_2+O_2 flows indicates that the chemical composition of the reactive mixture has a stronger effect than the relative reactivity of N_2 and O_2 (kinetically driven regime). This is because the O_2 content is still low in relation to the sputtered area of the Zr target. In Zone R, the Zr concentration is clearly reduced due to starting of poisoning effect on the target. In parallel, the O and N concentrations increase. Finally, in Zone P, the Zr concentration is similar to Zone R, but it is observed that the O concentration grows at expenses of N. This is because, in presence of enough N_2 and O_2, the preferential affinity of Zr towards O begins to dominate (thermodinamically driven regime).

The different sputtering modes have also a clear influence on the growth mode of the coatings, as observed in the SEM cross section micrographs of the films displayed in Figure 2. The different types of growth are indicated in Table 1 as well. In agreement with Figure 1b, it is very clear that the first couple of films have a considerable higher thickness than the others (Figure 2a and b). These images reveal a columnar morphology, which is typical for films deposited by DC magnetron sputtering. The columns became narrower and more defined for higher

mixture flows. Sample F4.75 (Figure 2d), in the border of Zones R and P, shows a change of microstructure, where the column growth appears 'interrupted', and the columnar structure starts to vanish. Further increase of flow of mixture leads to denser featureless compact microstructures (Figures 2e and f). In general, the variation of growth corresponds with the zones defined in Figure 1. In fact, this evolution from columnar to a more dense structure with the increase of the gas flow is similar to what was reported by other authors [6, 8, 16, 35, 37, 50, 51]. It is worth mentioning that the mass density variations included in Table 1 seem to be mainly related to the variation of phase composition, as indicated before. Nevertheless, the atomic density obtained from RBS is higher on films with O, being the maximum on sample F4.25, in agreement with the trend observed by SEM.

3.2. Variation of the N_2+O_2 flow: chemical composition and crystallographic phases

The chemical composition of the different films is plotted in a ternary diagram in Figure 3. A line connecting Zr_3N_4 and ZrO_2 is included for reference, since it probably represents a 'limit' where more O and N cannot be stabilized by Zr [24]. In fact, in the line connecting these latter two compounds we can find other four oxynitride phases (Zr_2ON_2, $Zr_7O_8N_4$, $Zr_7O_{9.5}N_3$ and $Zr_7O_{11}N_2$) [52–56], which are chemically related with the oxide and nitride by:

$Zr_3N_4 + ZrO_2 \rightarrow 2\ Zr_2ON_2$

$Zr_3N_4 + 4\ ZrO_2 \rightarrow Zr_7O_8N_4$

$3\ Zr_3N_4 + 19\ ZrO_2 \rightarrow 4\ Zr_7O_{9.5}N_3$

$Zr_3N_4 + 11\ ZrO_2 \rightarrow 2Zr_7O_{11}N_2$

All the relevant phases are included in Figure 3 as stars.

The first observation that can be made is that the samples are located in a small area of the diagram, in a similar region of other works from literature [3, 8, 12, 16, 18–20, 22–25, 33, 34, 37–39, 51, 57, 58]. Most of them are situated near the band that connects ZrN to ZrO_2, although not reaching compositions close to ZrO_2. This is because the flow of reactive gas was restricted to values where intrinsic colored coatings were obtained. An excess of O content would lead to transparent films, within the visible region of the electromagnetic spectrum, and the eventually obtained colors would be resultant of interference effects. The samples where the

N_2+O_2 flow was varied are plotted as black circles connected by a black line. The films can be divided into three groups, in agreement with Figure 1c. Therefore, for low flows, the samples are close to the Zr-N edge and to the Zr vertex. For higher flows, a group of three samples is located between the ZrN and the Zr_2ON_2, while samples produced with highest flows are displaced to higher O concentrations with respect to them.

The chemical composition of the samples has a strong influence on their crystalline structure, as can be observed in Figure 4a. The films can also be divided into three groups (labelled as 1, 2 and 3 in Table 1), according to the general shape of the diffractograms. The first group is formed by the two with highest Zr content, and it is characterized by the appearance of broad peaks whose position agrees with the c-ZrN. The broadness of the peaks may be correlated with the relatively distorted crystallites due to deficiency of N relatively to stoichiometric ZrN. The (111) is clearly detected in both films, and the (200), (220) and (311) appear more or less clearly in sample F3.75, indicating the formation of a c-ZrN-like structure. It is worth mentioning that one peak whose position fits with the (211) of bcc c-Zr [ref. 01-089-4916] is observed at ca. 63º on film F2.50, which agrees with the high concentration of Zr in this sample. Clearly, these films are distinguished by a poorly-formed c-ZrN due to the low N concentration (cf. Figure 1c and Figure 3).

In contrast, the three samples belonging to the second group are characterized by sharp well-formed peaks. In case of sample F4.00, all the peaks can be identified as c-ZrN. In the other two samples, additional peaks are observed, whose positions fit with c-Zr_2ON_2. These phases are in good agreement with the position of these samples in the ternary diagram (cf. Figure 3). Finally, the third group shows band-shaped peaks, whose positions agree with c-ZrN, when observable. Since these samples have higher O content than the previous, it can be stated that the introduction of additional oxygen beyond the formation of c-Zr_2ON_2 led to a strong distortion of the crystalline structure of the films. The incorporation of oxygen in the zirconium nitride structure, forming a Zr-O-N phase (ZrN and ZrO are isostructural), would cause its deformation and higher number of defects promoting the amorphization, which explains the broadening of the peaks. It is important to note that even higher values of N_2+O_2 flows leads to disappearance of peaks and further amorphization of the structure. In addition, the peak (111) is not centred

around the position of the c-ZrN or c-ZrO, but it is broadened to lower angles and also covers the region of the peaks of the c-Zr_2ON_2 phase that appeared for the films belonging to group 2. Therefore, this can be interpreted as the result of growth and distortion of the c-Zr_2ON_2 peaks observed in group 2, or the appearance of a new phase (e.g. Zr_3N_4 or m-ZrO_2) [3, 5, 6, 8, 9, 14, 16, 18–29, 31–41, 43–46, 51, 58, 59].

These results are similar to what has been studied in literature for reactively sputtered Zr-O-N films. Signore et al. [31], Rizzo et al. [32] and Carvalho et al. [12, 13] observed the change in the ZrN preferred orientation from (111) to (200) with the increase of the reactive gas flow, and Huang et al. [16, 18] reported ZrN (111) preferred orientation with the presence of (200) and (220) peaks at low O flows. The results indicate that the preferred orientation is determined by the lowest energy plane, which is a process that consists in a competition between the plane with lowest strain energy (111) and the plane lowest surface energy (200) [60]. In our case, the c-ZrN phase show strong (111) preferred orientations first, and new peaks belonging to c-ZrN appear at N/Zr ratios approaching stoichiometry. In addition, Ngaruiya and Venkataraj [28–30], Huang et al. [19], Chan et al. [34] observed the evolution from ZrN to ZrN_xO_y-type (and even to ZrO_2) structures with further increase of the reactive flow.

3.3. Variation of the N_2+O_2 flow: color

The films deposited with a N_2+O_2 flow higher than 5.0 sccm show non-intrinsic color and therefore are excluded from the plot of color coordinates depicted in Figure 5. These films are not opaque but show some color, except the film deposited with 15 sccm which is fully transparent (further details can be found in a dedicated paper [61]).In fact, film F4.75 is somehow in the limit, showing bluish color but also a certain degree of transparency. This is the reason why is connected with dashed lines to the other samples, which share a common trend. This trend is located in a similar region than other samples in literature [6, 13, 14]. The characteristics of the different steps of this common trend are summarized in Table 2; for low values of N_2+O_2 flows (high metal contents, Group 1 in XRD), the films show silver color. The increase of flow of the mixture leads to golden and dark

golden films (Zr/N ratios around 1 and Group 2 in XRD), although the values of L* are lower than samples reported in literature for such colors [6, 14]. A further increase of N_2+O_2 flow (samples with higher amount of O and Group 3 in XRD) leads to bluish and non-intrinsic colors.

3.4. Further exploration of the deposition parameter space

For this investigation, films belonging to Zone P were not selected due to their lack of intrinsic color. New sets of films were produced by maintain the parameters of the reference films but varying the Ar flow, or the target voltage, or the bias or the deposition time (see Table 1).

The increase of Ar flow from 25 to 40 sccm (from F4.25 to F4.25-Ar40) caused a logical increase of pressure and reduction of target voltage, and the opposite is seen for its reduction from 25 to 10 sccm (from F4.25 to F4.25-Ar40). However, the magnitude of the variation is different, and the changes observed for the Ar flow reduction are clearly larger, which will be reflected in the variation of the characteristics and properties of the films. Remarkably, in both cases the chemical composition shows an increase of Zr content, which is stronger in the case of film produced with lower Ar flow, F4.25-Ar10 (see Figure 3). A reduction of N content is also observed. The deposition rate of F4.25-Ar40 is significantly larger relatively to the reference film (F4.25) while in case of F4.25-Ar10 is slightly lower. In addition, the XRD diffractograms reflect a shift towards Group 1 (see Figure 4). In case of F4.25-Ar40 the modification is smaller, and only the disappearance of the c-Zr_2ON_2 peaks is observed. In contrast, F4.25-Ar10 moves to Group 1, and only the (111) peak of c-ZrN is visible. As a consequence of these modifications, the color of the films changes from dark golden to silver (Figure 5), as observed previously in the samples with low N_2+O_2 flow. Nevertheless, film F4.25-Ar40 shows an abnormally low value of coordinate L* (see Figure 5a), which probably indicates that this sample is in an intermediate situation between the nitride and the metallic region.

The reduction of target current causes an increase of pressure (and the opposite for the increase), indicating that a change of the sputtering regime has taken place. The increase of pressure is higher for lower N_2+O_2 mixture flow (e.g. higher variation from F3.75 to F3.75-I1.5 than from F4.25 to F4.25-I1.5, see Table 1),

which is an indication of stronger change of sputtering mode. On the one hand, the increase of target current to 2.5 A causes a variation similar to the reduction of the Ar flow (close points in the ternary diagram in Figure 3 and similar diffractograms in Figure 4); thus, the thickness is more or less invariant, but the Zr concentration is increased, leading to XRD diffraction belonging to Group 1 and exhibiting silver color (Figure 5). On the other hand, the reduction of target current to 1.5 A induces the deposition to the poisoned mode. Thus, the thickness is dramatically reduced, the O concentration is high and the XRD plots belong to Group 3. Such move to poisoned mode is especially relevant for sample F3.75-I1.5, since F3.75 was a representative of the 'metallic' mode. Such change causes a reduction of mass density due to the reduction of Zr content, but an increase of atomic density due to the densification of the structure. Nevertheless, F3.75-I1.5 shows the chemical composition closer to the previous samples of Group 3 in the ternary diagram (cf. Figure 3), and also an 'interrupted' growth (SEM image not shown), indicating that although prepared in poisoned mode, it is close to the boundary. It should be emphasized that the three films produced with lower current appear 'ordered' following higher flows of N_2+O_2, showing progressively higher O contents (Figure 3) and XRD patterns indicative of more amorphous films (Figure 4), respectively. As expected considering the chemical compositions and XRD results, all these films are transparent.

The application of substrate bias does not cause any relevant variation in deposition pressure, and the deposition rate and growth modes are kept invariant. However, it has been found that the target voltage increased in both cases, probably leading to higher Zr concentrations and lower N contents. The XRD's are similar to the unbiased sample (Group 2 with presence of c-Zr_2ON_2). Nevertheless, in case of F4.25-B30 peaks of the oxynitride phase between 60 and 65º could be clearly detected, which were only incipient in the reference film F4.25. The color of the sample deposited with 30 V of bias does not show any major change, but F4.25-B40 showed a reduction of L* and b* coordinates, moving to the 'red-brownish' region.

Finally, the deposition time does not cause any strong variation of the deposition parameters. The deposition pressure is similar (reactive mode), and the diffractograms belong to Group 2. However, it can be noted that target voltage

shows a consistent reduction with deposition time, indicating that the reactive system evolves with time. Thus, both samples F4.50-t30 and F4.50-t120 show higher Zr contents than F4.50 at expenses of N and O, respectively. In fact, F4.50-t120 shows a diffractogram only composed by peaks of c-ZrN, in agreement with its chemical composition close to ZrN (see Figure 3). The color of the films is displaced to different directions in Figure 5, in agreement with the opposite variations in chemical compositions; thus, while the sample deposited with 30 minutes moved towards light-golden direction, the film deposited for 120 min showed red-brownish color.

In general, it can be stated that Ar flow and target current caused stronger variations in the sputtering mode, XRD group and chemical composition of the films. This was reflected in color displacements to the limits of the scale, to silver (metallic-like) and transparent (oxide-like). The modifications introduced by bias and deposition time were less intense, and the sputtering mode and XRD group were not modified. Only the appearance or disappearance of peaks could be detected. As a consequence, the color changes were not so deep, and varied in a region close around the color of the original film.

3.5. Mechanical properties

The mechanical properties of the films have been evaluated on representative samples belonging to each of the groups identified so far: type M, with poorly formed c-ZrN (F3.75); type R, with well formed c-ZrN (F4.00), or including also c-Zr_2ON_2 (F4.25); type P, with amorphous structure (F4.75). Since bias is expected to have an influence on the mechanical properties, film F4.25-B40 has been also measured. Figure 6 shows the indentation curves obtained for all these films. Three of the films show similar loading curves (although the biased film is a little bit displaced to lower displacements), while in the other two cases (F3.75 and F4.75) the curves are clearly displaced to higher displacements at a given load. This indicates that those latter films, which represent the groups of samples deposited in metallic and poisoned mode, respectively, will show lower values of mechanical properties. Such observation can be confirmed in Figure 7, where hardness, reduced Young's modulus and elastic work are represented against reactive flow.

The elastic work is similar for all the films around 50%. In contrast, hardness and reduced Young's modulus shows similar trends, which can be explained through the type and quality of phases present in the films. The first increase of reactive flow leads to the increase of H and E*, which is probably caused by the formation of a well-crystallized c-ZrN-like structure. Then, the appearance of c-Zr_2ON_2 phase at flow of 4.25 sccm seems to reduce slightly both parameters. Finally, with the amorphization of the structure leads to a dramatic drop of both hardness and Young's modulus. It is also worth mentioning that biasing leads to a moderate hardness increase, as it was expected.

In general, the values of mechanical properties are not very large, which can be expected for columnar films deposited in reactive DC sputtering. In addition, the presence of relatively large amounts of O is known to reduce the mechanical properties of ZrN [14]. Nonetheless, observed values are still reasonable for decorative applications; in addition, relatively low Young's modulus favours the matching with conventional underlying substrates, reducing the presence of undesired stresses at the interface.

4. Conclusions

Zr-O-N films from literature occupy a very similar region of the ternary diagram, near the Zr-N edge and then around the line connecting Zr_3N_4 and ZrO_2. The aim of this work is to evaluate the stability of the Zr-O-N system by studying the impact of the variation of different deposition parameters on the characteristics and properties of Zr-O-N films, aiming at decorative applications.

The reference series prepared by variation of N_2+O_2 flow led to a modification from metallic (Zr-rich poorly formed c-ZrN) to reactive (well-formed c-ZrN with or without c-Zr_2ON_2) and to poisoned regimes (high oxygen content and amorphous nature). These changes could be well correlated with the sputtering parameters. From that generic trend, the different parameters studied showed different effects. The variations of Ar flow and Zr target current caused stronger changes, while bias and deposition time caused moderate variations. The color of the samples all laid in the same region, although slightly different from what has been observed in literature. The mechanical properties are reasonable for decorative applications. Both

properties could be well explained according to the different phases present in the films. The Zr-O-N system appears to be very stable, and therefore other synthesis strategies will be explored in order to reach new regions of composition.

Acknowledgements

The financial support of Portuguese Foundation of Science and Technology (FCT), under the project number IF/00671/2013 is gratefully acknowledged.

References

1. Piegari A, François F (2013) Optical thin films and coatings. Woodhead Publishing Limited

2. Vaz F, Cerqueira P, Rebouta L, et al (2004) Structural, optical and mechanical properties of coloured TiNxOy thin films. Thin Solid Films 447–448:449–454. doi: 10.1016/S0040-6090(03)01123-4

3. Ariza E, Rocha LA, Vaz F, et al (2004) Corrosion resistance of ZrNxOy thin films obtained by rf reactive magnetron sputtering. Thin Solid Films 469–470:274–281. doi: 10.1016/j.tsf.2004.08.091

4. Ariza E, Rocha LA, Ferreira SC, et al (2004) Corrosion behaviour of single layered ZrNx O y thin films in artificial sweat solutions. Proc. Eur. Corros. Conf.

5. Vaz F, Carvalho P, Cunha L, et al (2004) Property change in ZrNxOy thin films: Effect of the oxygen fraction and bias voltage. Thin Solid Films 469–470:11–17. doi: 10.1016/j.tsf.2004.06.191

6. Carvalho P, Vaz F, Rebouta L, et al (2005) Structural , electrical , optical , and mechanical characterizations of decorative ZrOxNy thin films. J Appl Phys 98:1–8. doi: 10.1063/1.1990261

7. Fernandes AC, Cunha L, Moura C, et al (2008) TiN-based decorative coatings : colour change by addition of C and O. J Optoelectron Adv Mater 10:900–903.

8. Moura C, Carvalho P, Vaz F, et al (2006) Raman spectra and structural analysis in ZrOxNy thin films. Thin Solid Films 515:1132–1137. doi: 10.1016/j.tsf.2006.07.039

9. Mohamed S, Abd El-Rahman A, Ahmed M (2007) Investigation of zirconium oxynitride thin films deposited by reactive pulsed magnetron sputtering. J Phys D Appl Phys 40:7057–7062. doi: 10.1088/0022-3727/40/22/029

10. Rezek J, Vlček J, Houška J, Čerstvý R (2014) High-rate reactive high-power impulse magnetron sputtering of Ta-O-N films with tunable composition and properties. Thin Solid Films 566:70–77. doi: 10.1016/j.tsf.2014.07.033

11. Belosludtsev A, Houška J, Vlček J, et al (2017) Structure and properties of Hf-O-N films prepared by high-rate reactive HiPIMS with smoothly controlled composition. Ceram Int 43:5661–5667. doi: 10.1016/j.ceramint.2017.01.102

12. Carvalho P, Chappé JM, Cunha L, et al (2008) Influence of the chemical and electronic structure on the electrical behavior of zirconium oxynitride films. J Appl Phys 103:104907. doi: 10.1063/1.2927494

13. Carvalho P, Borges J, Rodrigues MS, et al (2015) Optical properties of zirconium oxynitride films: The effect of composition, electronic and crystalline structures. Appl Surf Sci 358:660–669. doi: 10.1016/j.apsusc.2015.09.129

14. Carvalho P, Vaz F, Cunha L, et al (2005) Structural and Optical Characterization of Decorative ZrOxNy Thin Films. In: Soc. Vac. coaters -

Annu. Tech. Conf. Proc. pp 580–583

15. Cubillos GI, Olaya JJ, Clavijo D, et al (2013) Synthesis and biological characterization of zirconium oxynitride thin film growth by radio-frequency sputtering. Thin Solid Films 529:342–346. doi: 10.1016/j.tsf.2012.06.018

16. Huang J-H, Chang K-H, Yu G-P (2007) Synthesis and characterization of nanocrystalline ZrNxOy thin films on Si by ion plating. Surf Coatings Technol 201:6404–6413. doi: 10.1016/j.surfcoat.2006.12.007

17. Cubillos GI, Bethencourt M, Olaya JJ (2015) Corrosion resistance of zirconium oxynitride coatings deposited via DC unbalanced magnetron sputtering and spray pyrolysis-nitriding. Appl Surf Sci 327:288–295. doi: 10.1016/j.apsusc.2014.11.168

18. Huang JH, Tsai ZE, Yu GP (2008) Mechanical properties and corrosion resistance of nanocrystalline ZrNxOy coatings on AISI 304 stainless steel by ion plating. Surf Coatings Technol 202:4992–5000. doi: 10.1016/j.surfcoat.2008.05.001

19. Huang J-H, Lin T-C, Yu G-P (2011) Phase transition and mechanical properties of ZrNxOy thin films on AISI 304 stainless steel. Surf Coatings Technol 206:107–116. doi: 10.1016/j.surfcoat.2011.06.051

20. Huang J-H, Hu Y-Y, Yu G-P (2011) Structure evolution and mechanical properties of ZrNxOy thin film deposited on Si by magnetron sputtering. Surf Coatings Technol 205:5093–5102. doi: 10.1016/j.surfcoat.2011.05.015

21. Laurikaitis M, Burinskas S, Dudonis J, Milčius D (2008) Physical properties of zirconium oxynitride films deposited by reactive magnetron sputtering. J Phys Conf Ser 100:82051. doi: 10.1088/1742-6596/100/8/082051

22. Rawal SK, Chawla AK, Chawla V, et al (2010) Structural, optical and hydrophobic properties of sputter deposited zirconium oxynitride films. Mater Sci Eng B Solid-State Mater Adv Technol 172:259–266. doi: 10.1016/j.mseb.2010.05.027

23. Rawal SK, Chawla AK, Chawla V, et al (2011) Characterization of bi-phased Zr2ON2-ZrO2 coatings deposited by RF magnetron sputtering. Thin Solid Films 520:1589–1596. doi: 10.1016/j.tsf.2011.09.010

24. Rawal SK, Chawla AK, Jayaganthan R, Chandra R (2014) The influence of various sputtering parameters on structural, wettability and optical properties of Zr2ON2 thin films. Mater Sci Eng B Solid-State Mater Adv Technol 181:16–23. doi: 10.1016/j.mseb.2013.11.003

25. Mohamed SH, Hadia NMA, Ali HM (2015) Effect of annealing on properties of decorative zirconium oxynitride thin films. Eur Phys J Appl Phys 69:30301. doi: 10.1051/epjap/2015140475

26. Cubillos GI, Olaya JJ, Bethencourt M, et al (2013) Synthesis and characterization of zirconium oxynitride ZrOxNy coatings deposited via unbalanced DC magnetron sputtering. Mater Chem Phys 141:42–51. doi: 10.1016/j.matchemphys.2013.04.012

27. Cubillos GI, Olaya JJ, Clavijo D, et al (2012) Corrosion resistance and

biocompatibility of zirconium oxynitride thin film growth by rf sputtering. Thin Solid Films 58:328–334. doi: 10.1016/j.tsf.2012.06.018

28. Venkataraj S, Kappertz O, Jayavel R, Wuttig M (2002) Growth and characterization of zirconium oxynitride films prepared by reactive direct current magnetron sputtering. J Appl Phys 92:2461–2466. doi: 10.1063/1.1498963

29. Ngaruiya JM, Kappertz O, Liesch C, et al (2004) Composition and formation mechanism of zirconium oxynitride films produced by reactive direct current magnetron sputtering. Phys Status Solidi Appl Res 201:967–976. doi: 10.1002/pssa.200306774

30. Venkataraj S, Severin D, Mohamed SH, et al (2006) Towards understanding the superior properties of transition metal oxynitrides prepared by reactive DC magnetron sputtering. Thin Solid Films 502:228–234. doi: 10.1016/j.tsf.2005.07.280

31. Signore M a., Rizzo a., Mirenghi L, et al (2007) Characterization of zirconium oxynitride films obtained by radio frequency magnetron reactive sputtering. Thin Solid Films 515:6798–6804. doi: 10.1016/j.tsf.2007.02.033

32. Rizzo A, Signore M, Mirenghi L, Di Luccio T (2009) Synthesis and characterization of titanium and zirconium oxynitride coatings. Thin Solid Films 517:5956–5964. doi: 10.1016/j.tsf.2009.03.131

33. Tomsah IBI (2013) Ellipsometric Evaluation of the Optical Constants of Zirconium Oxynitride Thin Films Deposited by Reactive Pulsed Magnetron Sputtering. Acta Phys Pol A 124:141–145. doi: 10.12693/APhysPolA.124.141

34. Chan MH, Wu PL, Lu FH (2010) Preparation of ZrNxOy films by magnetron sputtering using air as a reactive gas. Thin Solid Films 518:7300–7303. doi: 10.1016/j.tsf.2010.04.097

35. Zhan G, Liu J, Guo J, et al (2015) Electrical transport property of zirconium oxynitride thin film deposited by magnetron sputtering process. J Mater Sci Mater Electron 26:9188–9194. doi: 10.1007/s10854-015-3610-2

36. Carvalho P, Chappé JM, Cunha L, et al (2008) Influence of the chemical and electronic structure on the electrical behavior of zirconium oxynitride films. J Appl Phys 103:104907. doi: 10.1063/1.2927494

37. Ferreira SCC, Ariza E, Rocha LAA, et al (2006) Tribocorrosion behaviour of ZrOxNy thin films for decorative applications. Surf Coatings Technol 200:6634–6639. doi: 10.1016/j.surfcoat.2005.11.083

38. Macedo F, Carvalho P, Cunha LL, et al (2009) The Role of Modulated IR Radiometry Measurements in the Characterization of Zr-O-N Thin Films. Plasma Process Polym 6:760–766. doi: 10.1002/ppap.200931802

39. Carvalho P, Cunha L, Alves E, et al (2009) ZrOxNy Decorative Thin Films Prepared By the Reactive Gas Pulsing Process. J Phys D Appl Phys 42:195501. doi: 10.1088/0022-3727/42/19/195501

40. Cunha L, Vaz F, Moura C, et al (2006) Structural evolution in ZrNxOy thin

films as a function of temperature. Surf Coatings Technol 200:2917–2922. doi: 10.1016/j.surfcoat.2004.09.030

41. Carvalho P, Fernandes a. CC, Rebouta L, et al (2006) Compositional and structural changes in ZrOxNy films depending on growth condition. Nucl Instruments Methods Phys Res Sect B Beam Interact with Mater Atoms 249:458–461. doi: 10.1016/j.nimb.2006.03.031

42. Carvalho P, Vaz F, Rebouta L, et al (2005) Structural stability of decorative ZrNxOy thin films. Surf Coatings Technol 200:748–752. doi: 10.1016/j.surfcoat.2005.02.100

43. Signore MA, Rizzo A, Tapfer L, et al (2010) Effect of the substrate temperature on zirconium oxynitride thin films deposited by water vapour-nitrogen radiofrequency magnetron sputtering. Thin Solid Films 518:1943–1946. doi: 10.1016/j.tsf.2009.07.153

44. Rizzo A, Signore MA, Mirenghi L, et al (2010) Nano-crystalline Zr2ON2 thin films deposited by reactive magnetron sputtering. Surf Coatings Technol 204:2019–2022. doi: 10.1016/j.surfcoat.2009.10.031

45. Rizzo A, Signore MA, Mirenghi L, et al (2009) Physical properties evolution of sputtered zirconium oxynitride films: effects of the growth temperature. J Phys D Appl Phys 42:235401. doi: 10.1088/0022-3727/42/23/235401

46. Rizzo A, Signore MA, Mirenghi L, et al (2012) Sputtering deposition and characterization of zirconium nitride and oxynitride films. Thin Solid Films 520:3532–3538. doi: 10.1016/j.tsf.2012.01.005

47. Pascual-Izarra C, Reis MA, Barradas NP (2006) Simultaneous PIXE and RBS data analysis using Bayesian inference with the DataFurnace code. Nucl Instruments Methods Phys Res Sect B Beam Interact with Mater Atoms 249:780–783. doi: 10.1016/j.nimb.2006.03.190

48. Klein GA (2010) Industrial Color Physics, 1st ed. Springer, London

49. Oliver WC, Pharr GM (1992) An improved technique for determining hardness and elastic modulus using load and displacement sensing indentation experiments. J Mater Res 7:1564–1583. doi: 10.1557/JMR.1992.1564

50. Huang J, Best SM, Bonfield W, Buckland T (2010) Development and characterization of titanium-containing hydroxyapatite for medical applications. Acta Biomater 6:241–9. doi: 10.1016/j.actbio.2009.06.032

51. Huang J-H, Wu T-H, Yu G-P (2009) Heat treatment induced phase separation and phase transformation of ZrNxOy thin films deposited by ion plating. Surf Coatings Technol 203:3491–3500. doi: 10.1016/j.surfcoat.2009.05.016

52. Lerch M, Krumeich F, Hock R (1997) Diffusion controlled formation of β type phases in the system ZrO2-Zr3N4. Solid State Ionics 95:87–93. doi: 10.1016/S0167-2738(96)00549-8

53. Mazzoni AD, Conconi MS (2004) Study of carbonitriding reactions of zirconia. Synthesis of Zr(C,N,O) phases and ??-type zirconium oxynitrides.

Ceram Int 30:23–29. doi: 10.1016/S0272-8842(03)00057-9

54. Ohashi M, Yamamoto H, Yamanaka S, Hattori M (1993) Preparation and properties of zirconium oxynitrides by the reaction of zirconia with a layer structured zirconium nitrochloride. Mater Res Bull 28:513–521.

55. Lerch M, Rahäuser O (1997) Subsolidus phase relationships in the ZrO2-rich part of the ZrO2–Zr3N4 system. J Mater Sci 32:1357–1363. doi: 10.1023/A:1018521026557

56. Arvinte IR, Apreutesei M, Constantin D, et al (2010) Decorative aspects of ZrNx thin films prepared by reactive magnetron sputtering. 3:

57. Mohamed SH, Abd El-Rahman AM, Ahmed MR (2007) Investigation of zirconium oxynitride thin films deposited by reactive pulsed magnetron sputtering. J Phys D Appl Phys 40:7057–7062. doi: 10.1088/0022-3727/40/22/029

58. Chen YM, Liao B, Wu XY, et al (2013) Synthesis and characterization of zirconium oxynitride coatings deposited by filtered cathodic vacuum arc technology. Surf Coatings Technol 228:S210–S213. doi: 10.1016/j.surfcoat.2012.06.015

59. Laurikaitis M, Dudonis J, Milčius D (2008) Deposition of zirconium oxynitride films by reactive cathodic arc evaporation and investigation of physical properties. Thin Solid Films 516:1549–1552. doi: 10.1016/j.tsf.2007.03.063

60. Pelleg J, Zevin LZ, Lungo S (1991) Reactive sputter deposited TiN films on glass substrates. Thin Solid Films 197:117–128.

61. Oliveira CI da S, Martinez DM, Al-Rjoub A, et al (2017) Development of a statistical method to help evaluating the transparency/opacity of decorative thin films. Submitt. to Appl. Surf. Sci.

Figure captions

Figure 1. Influence of the reactive gas flow on different deposition and film parameters: a) Pressure and steady-state Zr target potential. b) Deposition rate; c) Chemical composition. The dashed lines represent the trends.

Figure 2. X-section SEM images of different Zr-O-N films. a) F2.50. b) F3.75. c) F4.25. d) F4.75. e) F5.00. f) F5.25. Scale bars represent 500 nm.

Figure 3. Ternary diagram showing the chemical composition of the different Zr-O-N samples studied. The reported crystalline phases are also included as stars. A straight line connecting the phases with lowest Zr content is depicted to show their relationship (see text for details).

Figure 4. X-ray diffraction patterns of different Zr-O-N films. a) Variation of the O_2+N_2 flow. b) Variation of Zr target current, voltage bias, Ar flow and deposition time.

Figure 5. Color of Zr-O-N films. a) Three-dimensional plot of the color coordinates of different films. The projections on the different planes is represented by hollow symbols. The line represents the overall trend, and the colors indicate the different zones (see Table 2). b) Bi-dimensional plot of the chromacity coordinates a* and b* on top of a color wheel. The lines connect the different symbols.

Figure 6. Nanoindentation curves of representative films of each group of samples (see Table 1).

Figure 7. Mechanical properties of representative films of each group of samples (see Table 1). The hollow symbol indicates the biased sample (-40 V).

Table 1. Deposition conditions and characteristics of the Zr-O-N films. The varying parameter in each sample is indicated in **bold**.

Film	Flow of gases (sccm)		Target current (A)	Bias (-V)	Deposition time (min)	Deposition pressure (Pa)	Target Voltage (V)	Thickness		Chemical composition (at. %)			Density		Zone*			
	N_2+O_2	Ar						SEM (nm)	RBS (10^{16} at/cm^2)	Zr	O	N	$\times10^{22}$ at/cm^3	g/cc	Sput.	XRD	SEM	Color
F2.50	**2.50**	25	2.0	0	60	0.35	275.5	1390	617	81.4	1.4	17.1	4.44	5.41	M	1	C	S
F3.75	**3.75**					0.37	276.7	1180	600	68.1	1.2	30.7	5.08	6.27	M	1	C	S
F4.00	**4.00**					0.38	297.6		576	45.6	10.7	43.7	-	-	R	2	C	G
F4.25	**4.25**					0.38	294.7	686	513	43.4	12.6	44.0	7.48	5.92	R	2	C	DG
F4.50	**4.50**					0.39	300.7	-	542	45.9	13.2	40.8	-	-	R	2	C	DG
F4.75	**4.75**					0.39	306.7	625	417	47.0	16.9	36.1	6.67	5.60	P	3	I	B-NI
F5.00	**5.00**					0.40		624	384	43.0	21.5	35.5	6.15	4.87	P	3	D	NI
F5.25	**5.25**					0.40		603	347	49.2	14.6	36.2	5.75	5.00	P	3	D	NI
F5.50	**5.50**						-	-	-	-	-	-	-	-	P	-	-	NI
F6.25	**6.25**					0.45	312.6	-	-	-	-	-	-	-	P	-	-	NI
F15.00	**15.00**					0.47	362.3	-	-	-	-	-	-	-	P	-	-	NI
F4.25-Ar10	4.25	**10**				0.20	367.8	-	498	55.5	7.5	37.0	-	-	M	1	-	S
F4.25-Ar40	4.25	**40**				0.45	289.3	-	729	46.8	13.0	40.3	-	-	R	2	-	S
F3.75-I1.5	3.75	25	**1.5**			0.40	285.5	418	275	41.9	23.9	34.2	6.58	5.12	P	3	I	NI
F4.00-I1.5	4.00		**1.5**			0.39	286.3	-	263	39.5	26.4	34.1	-	-	P	3	-	NI
F4.25-I1.5	4.25		**1.5**			0.39	296.2	-	304	35.8	30.1	34.1	-	-	P	3	-	NI
F4.25-I2.5	4.25		**2.5**			0.36	303.6	-	579	54.5	9.2	36.4	-	-	M	1	-	S
F4.25-B40	4.25		2.0	**40**		0.38	305.4	707	416	51.7	11.4	36.9	5.88	5.29	R	2	C	RB
F4.25-B30	4.25			**30**		0.39	297.8	-	454	52.4	7.3	40.3	-	-	R	2	-	DG
F4.50-t30	4.50			0	**30**	0.38	303.9	-	286	51.7	14.0	34.3	-	-	R	2	-	G
F4.50-t120	4.50				**120**	0.39	292.9	-	869	50.0	5.0	45.0	-	-	R	2	-	RB

**Sputtering modes: M (metallic), R(Reactive), P(Poisoned). Growth: C (Columnar), I (Interrupted columns), D (Dense). Color: S (Silver), G (Golden), DG (Dark Golden), RB (Red Brownish), B (Bluish), NI (Non Intrinsic).*

Table 2. Characteristics of the different trends observed in the representation of the color coordinates of Figure 5a. The invariant coordinates in each segment are indicated in **bold**, and the ranges of variation are indicated between parenthesis.

Sub trend	a*	b*	L*
Red	~0 → 5 (5)	~5 → ~30 (25)	~70 → ~63 (-7)
Green	~5 → ~10 (5)	~30 → ~20 (-10)	~63 → ~55 (-8)
Blue	**~10**	~20 → ~5 (-15)	~55 → ~50 (-5)
Pink	~10 → ~0 (-10)	~5 → ~-5 (-10)	**~50**

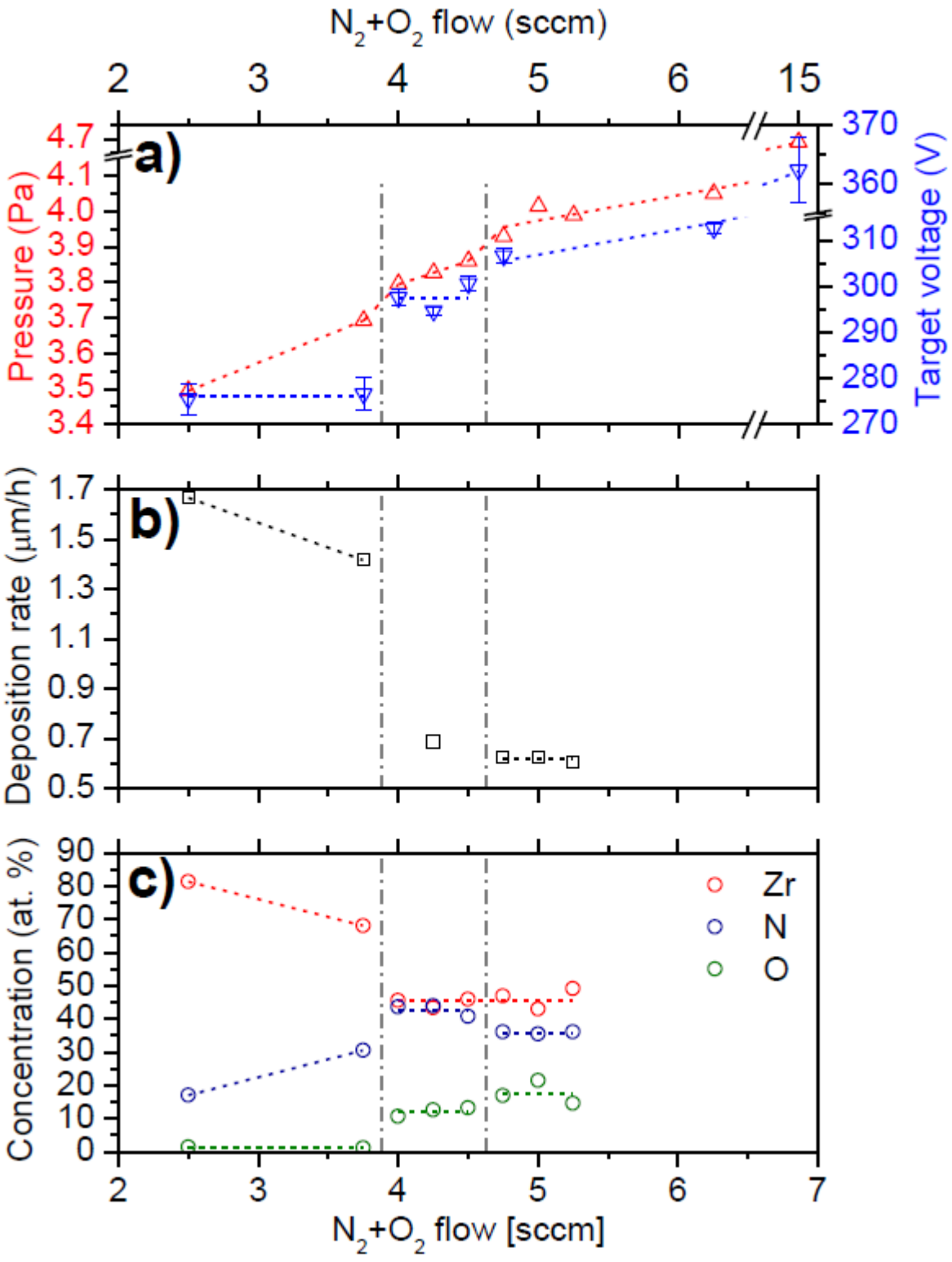

Fig. 1

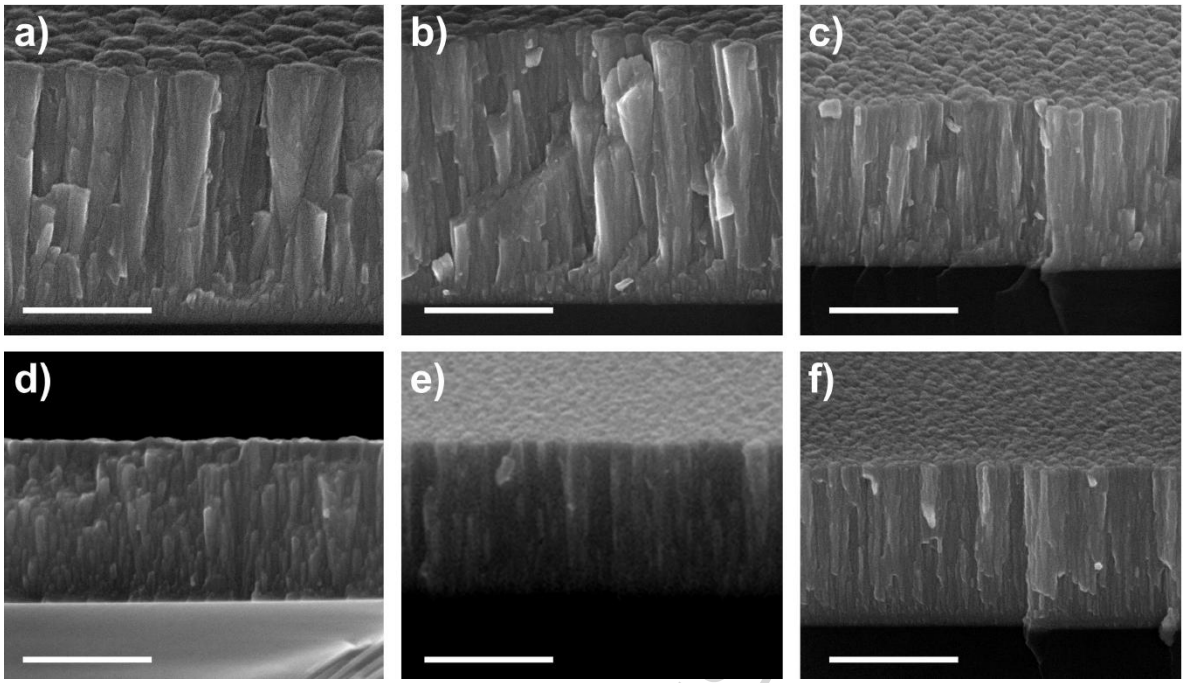

Fig. 2

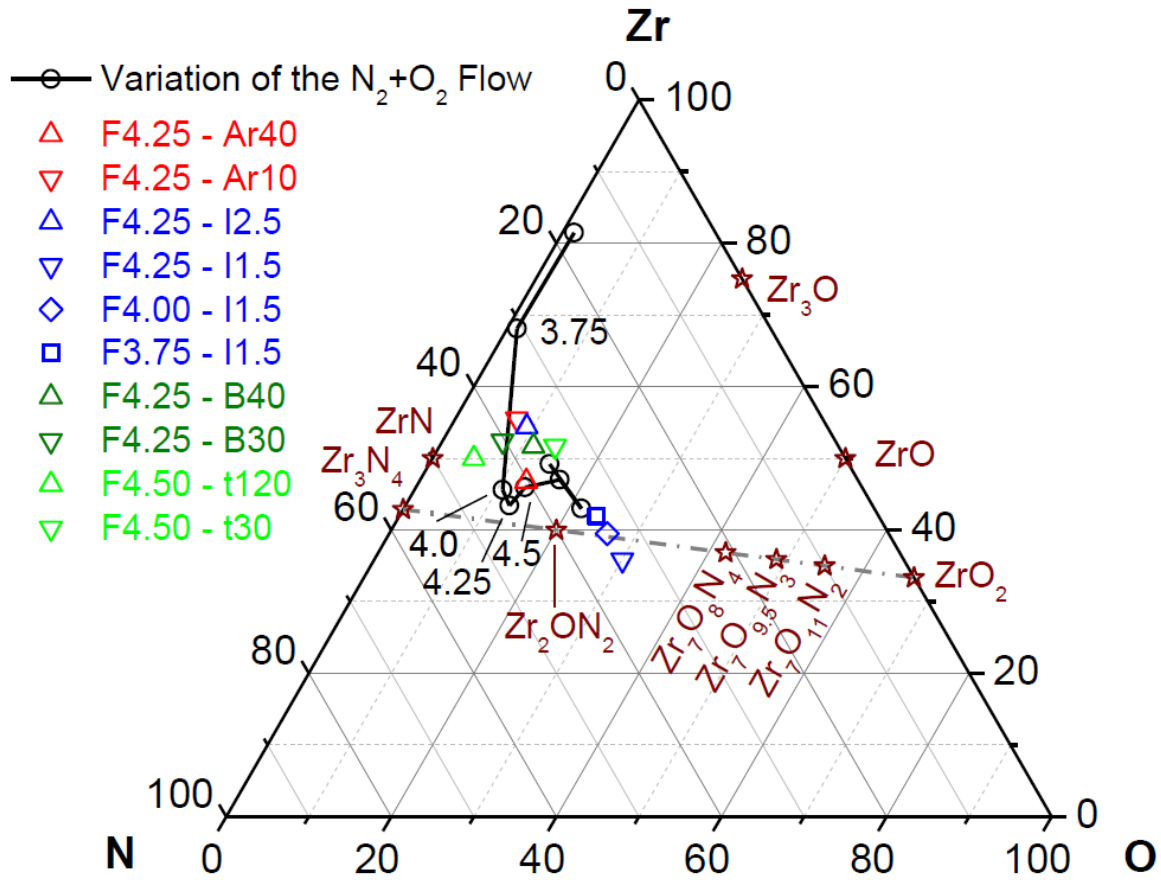

Fig. 3

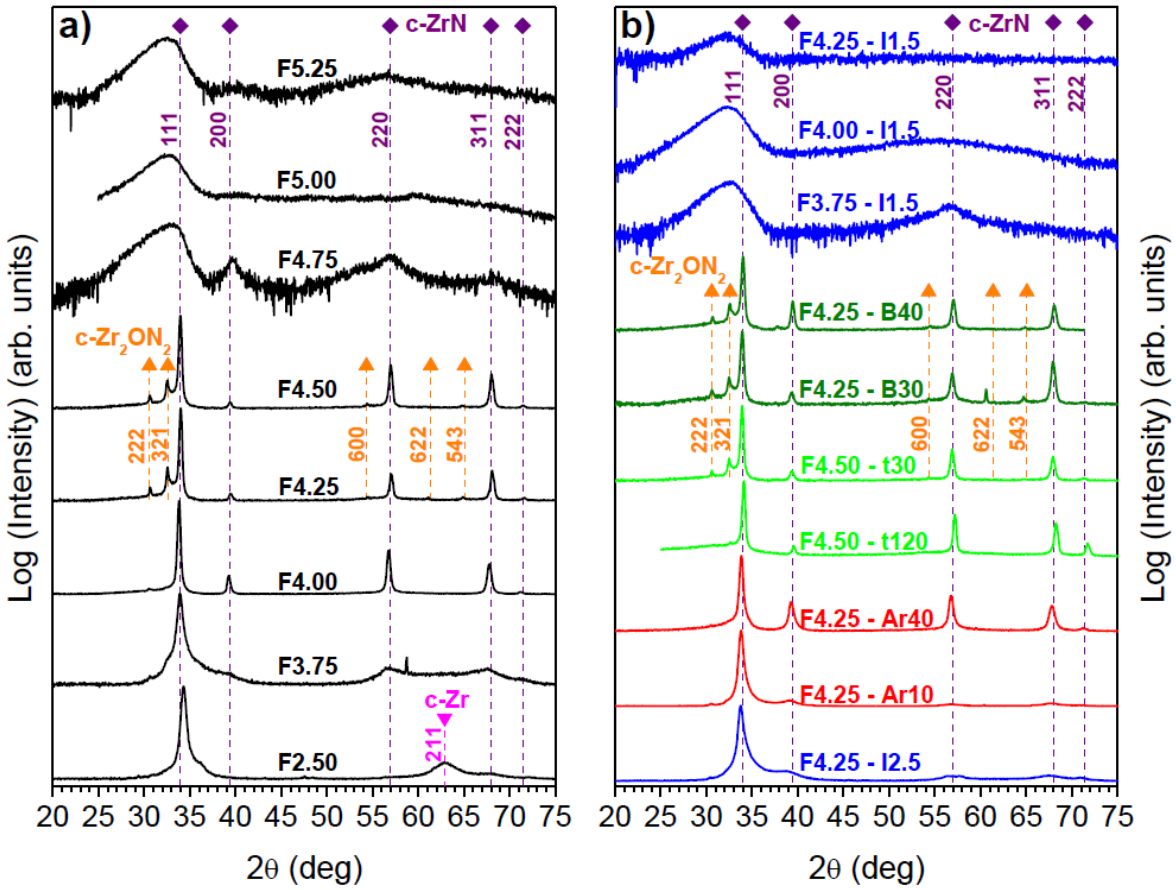

Fig. 4

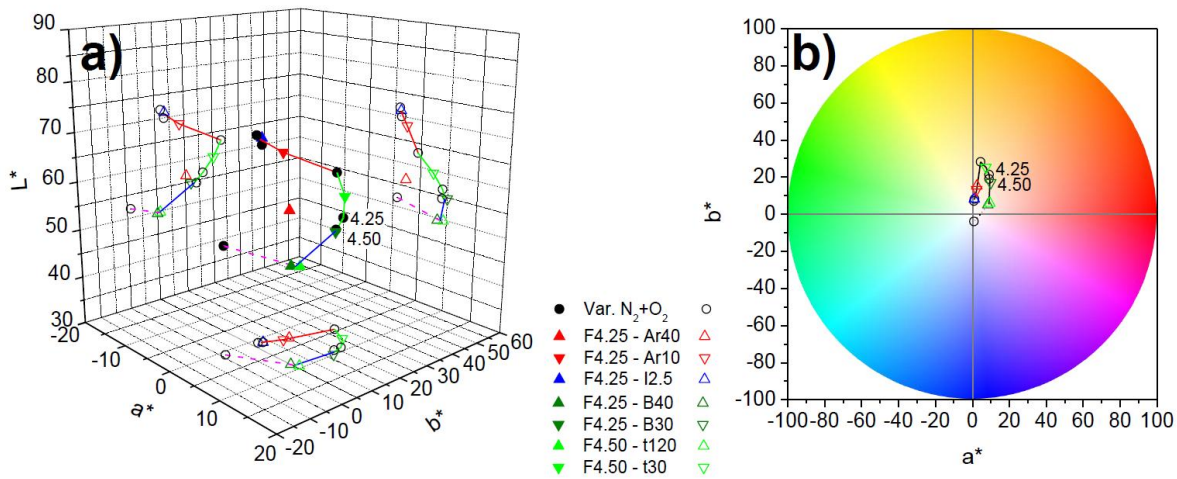

Fig. 5

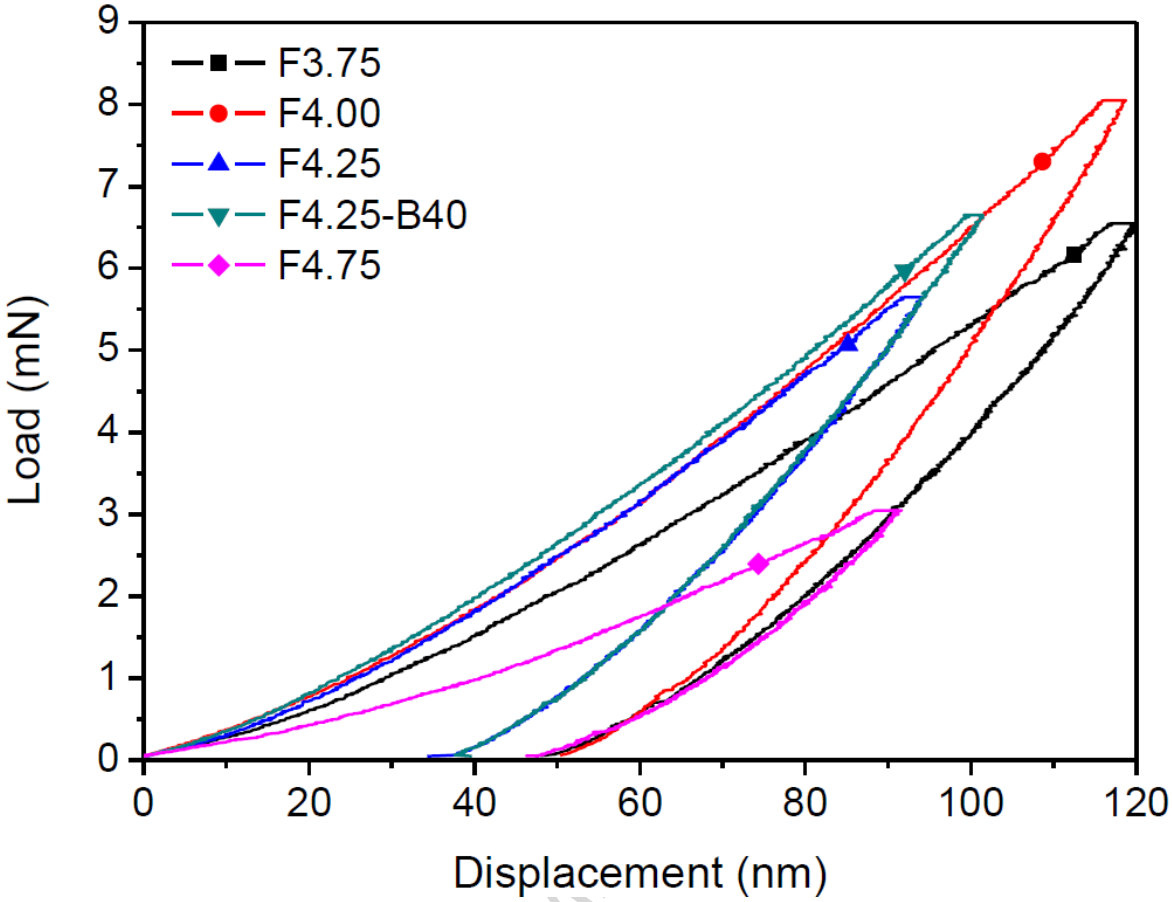

Fig. 6

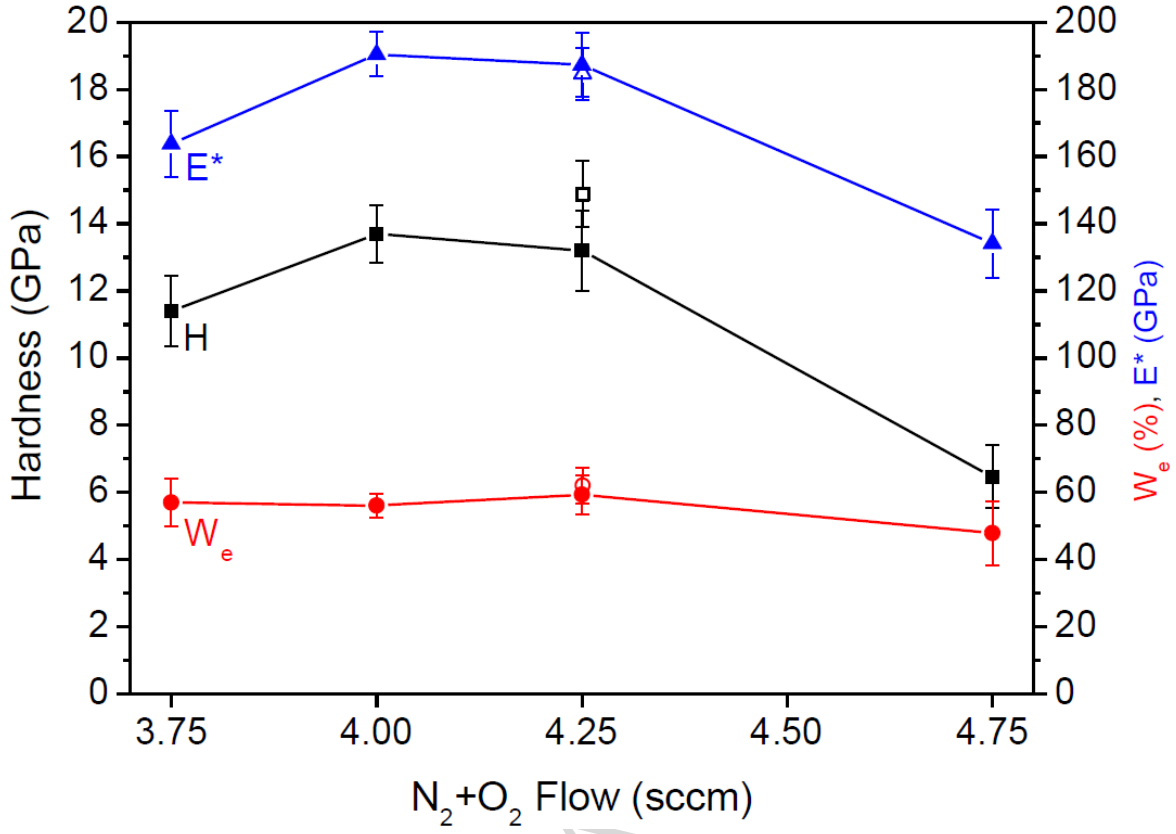

Fig. 7

Highlights

- The Zr-O-N system shows a very stable range of chemical compositions.
- Different deposition parameters have been varied to test such stability.
- Three regions of films are identified: Zr-ZrN, ZrN- Zr_2ON_2, disordered Zr-O-N.
- The color and mechanical properties of the films follows the phase composition.
- A different strategy is needed to avoid the verified chemical stability of the Zr-O-N system.